Table 2. Water isotope ratios ‰ ± 2 SEM. *, not measured.

Measurement	δD	$\delta^{18}O$
SAM-TLS atmosphere	4950 ± 1,080	*
SAM-TLS evolved water: Rocknest fines 230° to 430°C (*23*)	5880 ± 60	84 ± 10
Meteoritic crustal reservoirs (*26*)	~5000	*
Earth telescopes (*24*)	1700–8900	*
ALH 84001 (*17*)	3000	*
Shergotty USNM 321-1 (*17*)	4600	*

$\delta^{18}O$ values (*32*). These values are similar to the composition of the modern martian atmosphere, suggesting that the $\delta^{13}C$, δD, and $\delta^{18}O$ of the martian atmosphere were enriched early and have not changed much over ~4 billion years. Our higher values of δD and $\delta^{18}O$ measured in the atmosphere suggest that escape processes may have also continued since 4.0 Ga, in accordance with a two-stage evolutionary process (*17*) described above.

We observe large enrichments of $\delta^{18}O$ in atmospheric water vapor and CO_2. The $\delta^{18}O$ values of the water vapor are much larger than the $\delta^{18}O$ observed in carbonates and sulfates in martian meteorites and suggest that the oxygen in water vapor in the martian atmosphere is not in equilibrium with the crust (*33*, *34*) and could have been enriched in heavy isotopes through atmospheric loss. Another possibility is that the elevated oxygen isotope values in the more abundant martian CO_2 are being transferred to the water vapor through photochemical reactions in the atmosphere. However, $\delta^{18}O$ values of CO_2 in Earth's atmosphere are similarly elevated because of low-temperature equilibration between CO_2 and H_2O, and this process could also be operative on Mars (*12*).

In addition to atmospheric loss, other processes such as volcanic degassing and weathering might act to change the isotopic composition of the atmosphere through time. Estimates for the magnitude of these two contributions over the ~4-billion-year history of Mars vary widely (*30*, *34*, *35*), yet could have a strong impact on the isotopic composition of the atmosphere and challenge the status quo model described above.

References and Notes

1. P. R. Mahaffy *et al.*, *Space Sci. Rev.* **170**, 401–478 (2012).
2. J. P. Grotzinger *et al.*, *Space Sci. Rev.* **170**, 5–56 (2012).
3. P. R. Mahaffy *et al.*, *Science* **341**, 263–266 (2013).
4. C. R. Webster, P. R. Mahaffy, S. K. Atreya, G. J. Flesch, K. A. Farley, *Lunar Planet. Sci. Conf.*, abstract 1366 (2013).
5. B. M. Jakosky, R. J. Phillips, *Nature* **412**, 237–244 (2001).
6. M. B. McElroy, Y. L. Yung, A. O. Nier, *Science* **194**, 70–72 (1976).
7. T. Owen, J.-P. Maillard, C. de Bergh, B. L. Lutz, *Science* **240**, 1767–1770 (1988).
8. R. H. Carr, M. M. Grady, I. P. Wright, C. T. Pillinger, *Nature* **314**, 248–250 (1985).
9. V. A. Krasnopolsky, J. P. Maillard, T. C. Owen, R. A. Toth, M. D. Smith, *Icarus* **192**, 396–403 (2007).
10. P. B. Niles *et al.*, *Space Sci. Rev.* **174**, 301–328 (2013).
11. A. O. Nier, M. B. McElroy, *Science* **194**, 1298–1300 (1976).
12. P. B. Niles, W. V. Boynton, J. H. Hoffman, D. W. Ming, D. Hamara, *Science* **329**, 1334–1337 (2010).
13. R. E. Criss, *Principles of Stable Isotope Composition* (Oxford Univ. Press, Oxford, 1999).
14. C. R. Webster, A. J. Heymsfield, *Science* **302**, 1742–1745 (2003).
15. P. Hartogh *et al.*, *Nature* **478**, 218–220 (2011).
16. L. A. Leshin, S. Epstein, E. M. Stolper, *Geochim. Cosmochim. Acta* **60**, 2635–2650 (1996).
17. J. P. Greenwood, S. Itoh, N. Sakamoto, E. P. Vicenzi, H. Yurimoto, *Geophys. Res. Lett.* **35**, L05203 (2008).
18. J. Farquar, M. H. Thiemens, *J. Geophys. Res.* **105**, (2000).
19. C. S. Romanek *et al.*, *Nature* **372**, 655–657 (1994).
20. B. Jakosky, A. Zent, R. Zurek, *Icarus* **130**, 87–95 (1997).
21. H. R. Karlsson, R. N. Clayton, E. K. Gibson Jr., T. K. Mayeda, *Science* **255**, 1409–1411 (1992).
22. See the supplementary materials on *Science* Online.
23. L. A. Leshin *et al.*, *Lunar Planet. Sci. Conf.*, abstract 2220 (2013).
24. D. A. Fisher, *Icarus* **187**, 430–441 (2007) and references therein.
25. R. E. Novak *et al.*, *Bull. Am. Astron. Soc.* **35**, 660 (2005).
26. T. Usui, C. Alexander, J. Wang, J. Simon, J. Jones, *Earth Planet. Sci. Lett.* **357-358**, 119–129 (2012).
27. H. Lammer *et al.*, *Space Sci. Rev.* **174**, 113–154 (2013).
28. R. O. Pepin, *Icarus* **111**, 289–304 (1994).
29. L. Borg, M. J. Drake, *J. Geophys. Res.* **110**, E12S03 (2005).
30. P. B. Niles, L. A. Leshin, Y. Guan, *Geochim. Cosmochim. Acta* **69**, 2931–2944 (2005).
31. J. W. Valley *et al.*, *Science* **275**, 1633–1638 (1997).
32. J. Farquhar, D. T. Johnston, *Rev. Mineral. Geochem.* **68**, 463–492 (2008).
33. B. M. Jakosky, J. H. Jones, *Nature* **370**, 328–329 (1994).
34. M. Grott, A. Morschhauser, D. Breuer, E. Hauber, *EPSL* **308**, 391–400 (2011).
35. J. P. Bibring *et al.*, *Science* **312**, 400–404 (2006).
36. L. S. Rothman *et al.*, *J. Quant. Spectrosc. Radiat. Transf.* **110**, 533–572 (2009).

Acknowledgments: The research described here was carried out at the Jet Propulsion Laboratory, California Institute of Technology, under a contract with NASA.

Supplementary Materials

www.sciencemag.org/cgi/content/full/341/6143/260/DC1
Materials and Methods
Supplementary Text
Figs. S1 to S3
Tables S1 to S4
Reference (*37*)
MSL Science Team Authors and Affiliations

18 March 2013; accepted 17 June 2013
10.1126/science.1237961

Abundance and Isotopic Composition of Gases in the Martian Atmosphere from the Curiosity Rover

Paul R. Mahaffy,[1]* Christopher R. Webster,[2] Sushil K. Atreya,[3] Heather Franz,[1] Michael Wong,[3] Pamela G. Conrad,[1] Dan Harpold,[1] John J. Jones,[4] Laurie A. Leshin,[5] Heidi Manning,[6] Tobias Owen,[7] Robert O. Pepin,[8] Steven Squyres,[9] Melissa Trainer,[1] MSL Science Team†

Volume mixing and isotope ratios secured with repeated atmospheric measurements taken with the Sample Analysis at Mars instrument suite on the Curiosity rover are: carbon dioxide (CO_2), 0.960(±0.007); argon-40 (^{40}Ar), 0.0193(±0.0001); nitrogen (N_2), 0.0189(±0.0003); oxygen, 1.45(±0.09) × 10^{-3}; carbon monoxide, < 1.0 × 10^{-3}; and $^{40}Ar/^{36}Ar$, 1.9(±0.3) × 10^3. The $^{40}Ar/N_2$ ratio is 1.7 times greater and the $^{40}Ar/^{36}Ar$ ratio 1.6 times lower than values reported by the Viking Lander mass spectrometer in 1976, whereas other values are generally consistent with Viking and remote sensing observations. The $^{40}Ar/^{36}Ar$ ratio is consistent with martian meteoritic values, which provides additional strong support for a martian origin of these rocks. The isotopic signature $\delta^{13}C$ from CO_2 of ~45 per mil is independently measured with two instruments. This heavy isotope enrichment in carbon supports the hypothesis of substantial atmospheric loss.

The science and exploration goal of the Mars Science Laboratory (MSL) (*1*) is to advance our understanding of the potential of the present or past martian environments to support life. An understanding of how the present environment in Gale crater differs from the environment at the time of its formation requires comprehensive chemical characterization. The first set of experiments of the Sample Analysis at Mars (SAM) investigation (*2*) (Fig. 1) of the Curiosity rover included measurements of the chemical and isotopic composition of the atmosphere with sequences that employed two of SAM's three instruments. When

combined with composition and isotope data from atmospheric gases trapped in martian meteorites, measurements of the rate of atmospheric escape from orbiting spacecraft, and studies of atmosphere-surface exchange, SAM atmosphere measurements are intended to constrain models of atmospheric loss and climate evolution over geological time.

We report here on results from samples of the martian atmosphere analyzed by SAM's quadrupole mass spectrometer (QMS) and tunable laser spectrometer (TLS) during the first 105 sols (1 sol is a martian day) of the landed mission. These experiments were among the first carried out by SAM (Fig. 1) after several health checks of the instrument. The experiments took place over a period of several weeks from Mars solar longitude (*3*) of 163.7 to 211.2 (31 August to 21 November 2012) in Gale crater south of the equator (4.5°S, 137°E). All measurements were taken at night (table S1), and weighted means (table S2) are reported.

The mixing ratios of CO_2, N_2, Ar, O_2, CO, Ne, Kr, and Xe at the martian surface were determined by the mass spectrometers on the 1976 Viking Landers (*4*) more than 3 decades ago. Mass spectrometers on the Viking aeroshells also detected CO_2, N_2, Ar, CO, O_2, O, and NO (*5*) over an altitude range from 200 to 120 km, approaching or reaching the homopause or the altitude below which the atmosphere is well mixed. Spectroscopic measurements of CO have also been obtained from the Mars Reconnaissance Orbiter [e.g., (*6*)], the Mars Express Spacecraft (*7*, *8*), and a number of ground-based observations [e.g., (*9*)], revealing long-term variations correlated with solar activity (*9*). Recent Herschel submillimeter observations (*10*) have provided an additional measurement of the mixing ratios for CO (*10*) of $9.8(\pm1.5) \times 10^{-4}$ and for O_2 (*11*) of $1.40(\pm0.12) \times 10^{-3}$. The CO mixing ratio is found to vary by more than a factor of 4 (from $\sim 3 \times 10^{-4}$ to 1.2×10^{-3}) seasonally at polar latitudes, with smaller changes in the equatorial region (*6*). The relative change in CO reflects enrichment and depletion of noncondensable volatiles during the condensation and sublimation of CO_2, the principal component of the martian atmosphere.

Argon (^{40}Ar) has also been monitored globally from orbit by the gamma-ray spectrometer (GRS) on the Mars Odyssey spacecraft and from the martian surface by the alpha particle x-ray spectrometers (APXS) on the Mars Exploration rovers at latitudes of –2° and –15°. The GRS-derived Ar mixing ratio exhibits a large seasonal change by as much as a factor of 6 over the southern pole in winter (*12*) as the atmospheric CO_2 undergoes an annual cycle of condensation and sublimation, producing a 25% change in the surface pressure. Although the GRS data exhibit no seasonal change in Ar in the equatorial region (*12*), APXS finds that Ar nearly tracks the seasonal changes in surface pressure with a 2- to 3-month phase lag (*13*).

The mixing ratio of nitrogen can best be determined by in situ measurements because meteorite measurements do not give definitive answers for this atmospheric gas. Variations in isotopic composition of nitrogen in impact glasses of the martian shergotite meteorites EET79001 (*14*, *15*), Zagami (*16*), and Tissint [e.g., (*16*, *17*)] suggest that, in these samples, atmospheric nitrogen is mixed with an interior component with a lower $^{15}N/^{14}N$ ratio.

The atmospheric CO_2 isotope $\delta^{13}C_{VPDB}$ (VPDB, Vienna Pee Dee belemnite) (*18*) has been reported as –2.5 ± 4.3 per mil (‰) from the Thermal and Evolved Gas Analyzer (TEGA) mass spectrometer on the Phoenix lander (*19*) and as –22 ± 20 ‰ from Fourier transform Earth-based spectroscopy (*20*). The higher-uncertainty measurements of the Viking lander found CO_2 isotopes to be within 50‰ of terrestrial isotopes (*4*). The aeroshell measurements had similarly large error bars with reported carbon isotopic composition equivalent to $\delta^{13}C_{VPDB}$ of 23 ± 50‰ (*5*).

Detailed characterization of the SNC (Shergotty, Nakhla, and Chassigny) meteorites (*14*, *16*, *21*–*24*) has revealed a combination of volatile abundances and isotope systematics (*14*, *15*, *21*, *25*–*27*) for noble gases, N_2, and CO_2 that is possible only with origin on Mars or a very Mars-like parent body (*28*). Although the Viking abundance and isotope measurements provided evidence supporting the hypothesis that the SNCs are from Mars, the meteorites contain volatiles from other sources [for example, magmatic or possible cometary delivery (*29*)], in addition to trapped atmospheric gases that cause some variations among the meteorite values and differences between meteorite and Viking measurements. In addition to the uncertainties introduced by multiple sources of volatiles in the SNC meteorites, the solubility of the volatiles and their partitioning in glass and in the constituent mineral phases affects both the abundance value and the isotopic signature, including those of the noble gases (*30*, *31*). The SAM data are therefore key to constraining the atmospheric component of data obtainable from meteorites with in situ observations.

Many previous composition measurements analyzed only a single or a small number of species. The SAM instrument suite, with the use of

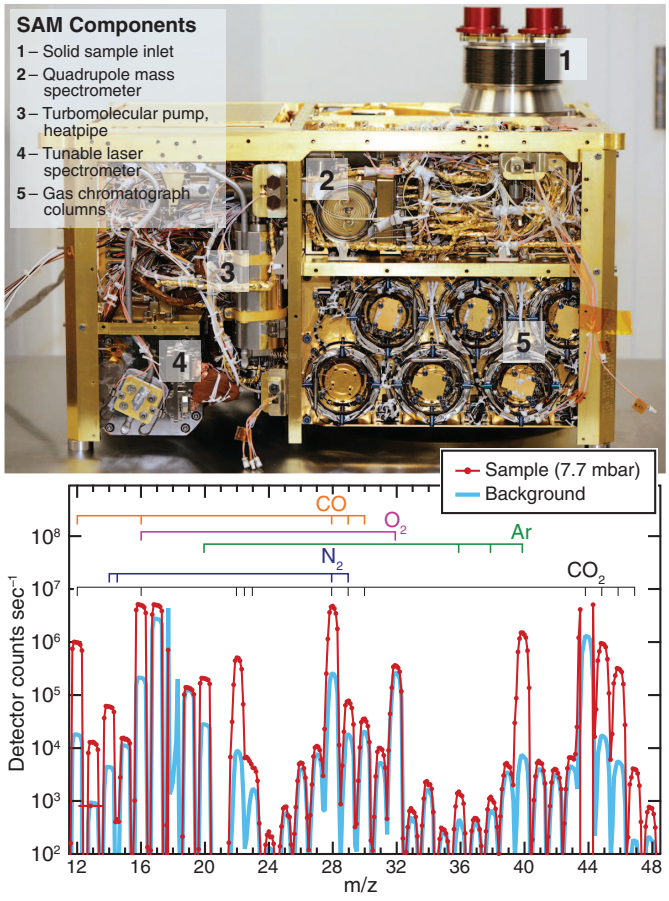

Fig. 1. The SAM suite located in the interior of the Curiosity rover uses three instruments to test either atmospheric gas or solid samples. (**Top**) An image of SAM with the side panels removed. (**Bottom**) Mass spectrum of the martian atmosphere from sol 45, with mass peaks labeled for the main atmospheric species. Isotopes of argon appear above the background level (blue traces) at mass/charge ratio (*m*/*z*) 36, 38, and 40 (green ticks at top of plot). Primary ions from isotopologues of CO_2, containing ^{13}C, ^{17}C, and/or ^{18}O, appear at *m*/*z* 45, 46, and 47 (black ticks at top of plot).

[1]NASA Goddard Space Flight Center, Greenbelt, MD 20771, USA. [2]Jet Propulsion Laboratory, California Institute of Technology, 4800 Oak Grove Drive, Pasadena, CA 91109, USA. [3]University of Michigan, Ann Arbor, MI 48109, USA. [4]NASA Johnson Space Center, Houston, TX 77058, USA. [5]Rensselaer Polytechnic Institute, Troy, NY 12180, USA. [6]Concordia College, Moorhead, MN 56562, USA. [7]University of Hawaii, Honolulu, HI 96822, USA. [8]University of Minnesota, Minneapolis, MN 55455, USA. [9]Cornell University, Ithaca, NY 14853, USA.

*Corresponding author. E-mail: paul.r.mahaffy@nasa.gov
†MSL Science Team authors and affiliations are listed in the supplementary materials.

Table 1. Volume mixing ratio measurements from Curiosity during the first 105 sols of the landed mission.

Gas	Volume mixing ratio (QMS)
CO_2	0.960(±0.007)
Ar	0.0193(±0.0003)
N_2	0.0189(±0.0003)
O_2	$1.45(\pm0.09) \times 10^{-3}$
CO	$<1.0 \times 10^{-3}$

Table 2. Isotopic composition measurements from Curiosity during the first 105 sols of the landed mission. N/A, not applicable.

Isotopes	Isotopic composition (QMS)	Isotopic composition (TLS)
$^{40}Ar/^{36}Ar$	$1.9(\pm0.3) \times 10^3$	N/A
$\delta^{13}C_{VPDB}$	45(±12) ‰*	46(±4) ‰†
$\delta^{18}O_{VPDB}$	N/A	48(±5) ‰

*$\delta^{13}C_{VPDB}$ is derived from *m/z* 12 and 13. †$\delta^{13}C_{VPDB}$, as derived from *m/z* 45 and 46, is described in the supplementary materials.

both the TLS and QMS, is able to make multiple, high-precision composition measurements over the course of the mission. In addition, SAM's QMS and TLS provide fully independent analyses of carbon isotopes. Repeat runs reported here were carried out at nearly the same time in the early evening on Mars to validate results. Each measurement set of the type implemented to date (*32*) represents a comprehensive analysis of the main constituents of the martian atmosphere.

SAM confirms the identity of the four most abundant gases in the martian atmosphere, with CO_2 being by far the major constituent. The SAM results for O_2 (Tables 1 and 2) are consistent with the recent Herschel (*11*) observations. SAM secures an upper limit for the CO mixing ratio (Tables 1 and 2) that is consistent with the Herschel data and the mean of all remote sensing spectroscopic measurements (~9×10^{-4}). Differences in CO mixing ratios are expected and are related to the abovementioned seasonal effects, as dynamics and mixing rather than chemistry are expected to dominate the behavior of CO in the homosphere due to the 3-year photochemical lifetime of CO. In addition to seasonal effects, localized, heterogeneous surface effects may also affect SAM measurements of CO because of possible adsorption of CO onto the surface during cold martian nights—when SAM data were collected—and reevaporation during warmer daytime. The Herschel observations, on the other hand, are weighted to higher in the atmosphere. Unlike CO, seasonal variation in O_2 has not yet been observed.

The most notable differences between the SAM measurements and previous data are in the relative abundances of Ar and N_2 and in the isotopic compositions of Ar and CO_2. The Ar/N_2 ratio and the N isotopes provide important constraints to models for assessing the relative contributions of internal and atmospheric sources to gas inclusions in shock-produced glassy martian meteorites. The isotope data are important for constraining models of atmospheric evolution. Whereas Viking found nitrogen and argon to be the second and third most abundant atmospheric gases at 2.7 and 1.6% by volume, respectively, SAM determines nearly equal volume mixing ratios for these constituents. Ar is found to be 21% greater, whereas N_2 is 30% lower than the Viking values. The resulting Ar/N_2 ratio of 1.02 measured by SAM is ~1.7 times greater than the value reported from Viking measurement (*4*). Both Ar and N_2 are noncondensable and practically inert gases on Mars, so their relative abundances are not expected to change considerably with time. We suspect that the difference from Viking results is due to different instrumental characteristics rather than some unknown atmospheric process, although seasonal variation in N_2 is yet to be tracked. The use on Mars of a turbomolecular pumping system (*33*), as well as repeated SAM analyses are expected to produce a more accurate determination of the ratio of these gases than the previous Viking in situ measurements whose mass spectrometers employed small ion pumps.

The SAM QMS offers independent validation of the $\delta^{13}C_{VPDB}$ value in CO_2 measured by the TLS (*34*). The average of three SAM QMS atmosphere measurements gives $\delta^{13}C_{VPDB}$ value of 45 ± 12 ‰, which is fully consistent with the independently measured TLS value of 46 ±4 ‰ (*34*). This observed ~5% enrichment in the heavier carbon isotope in the martian atmosphere compares well with previous measurements of ^{13}C-enriched carbon of atmospheric origin in martian meteorite EETA79001 (*22*, *35*). The data support the hypothesis that significant carbon has been lost from the martian atmosphere over time by sputtering (*36*).

The $^{40}Ar/^{36}Ar$ ratio of 1900 ± 300 measured by SAM is within error of the trapped atmosphere measured (*15*) to be 2050 ± 170 in quenched shock-produced melts in martian meteorite EETA79001 (*27*, *37*, *38*) but is considerably smaller than the value of 3000 ± 500 reported by Viking (*4*). Laboratory studies of shock implantation into silicate liquid have demonstrated that this process is a nearly quantitative recorder of atmospheric composition (*39*, *40*), and the implanted gases in meteorite shock-produced melts compared with the Viking in situ measurements of the atmosphere have been used as the best evidence to tie these meteorites to Mars (*14*, *15*, *21*, *41*). However, noble gases released from shock-produced glasses in EETA79001 contained at least three components (*27*): (i) martian air, (ii) terrestrial contamination, and (iii) a martian interior component with low $^{40}Ar/^{36}Ar$.

Even with the somewhat lower value measured by SAM, the $^{40}Ar/^{36}Ar$ of the martian atmosphere is highly elevated relative to the terrestrial ratio of 296. The enrichment in the radiogenic ^{40}Ar over nonradiogenic ^{36}Ar has been interpreted as evidence for significant loss of the primordial martian atmosphere early in the planet's history, followed by partial degassing of Ar. Subsequent loss to space is expected to lead to enrichment of the ^{40}Ar over ^{36}Ar (*42*, *43*) by the same processes that have reduced the $^{36}Ar/^{38}Ar$ ratio in the martian atmosphere. The latter ratio as inferred from EETA79001 glasses (*15*, *38*) was found to be ~4, much different from the terrestrial, chondritic, solar, and jovian (*44*) values which range in order from 5.3 to ~5.5. It is notable that the $^{40}Ar/^{36}Ar$ ratio has not changed appreciably since the ejection of EETA79001 from the planet ~700,000 years ago. This provides a constraint on the extent of very recent inputs of gas to the atmosphere from volcanic or cometary sources. The carbon dioxide isotope data support the hypothesis that a significant amount of carbon has escaped from the martian atmosphere over time, resulting in preferential loss of the lighter isotope of carbon and the observed enrichment in ^{13}C (*45*). This implies that atmospheric escape has dominated over exchange with unfractionated surface reservoirs that exist in the crust or mantle.

References and Notes

1. J. P. Grotzinger *et al.*, *Space Sci. Rev.* **170**, 5–56 (2012).
2. P. R. Mahaffy *et al.*, *Space Sci. Rev.* **170**, 401–478 (2012).
3. A Mars solar longitude of 180° represents the southern spring equinox, where the southern polar region would be covered with carbon dioxide ice.
4. T. Owen *et al.*, *J. Geophys. Res.* **82**, 4635–4639 (1977).
5. A. O. Nier, M. B. McElroy, *Science* **194**, 1298–1300 (1976).
6. M. D. Smith, M. J. Wolff, R. T. Clancy, S. L. Murchie, *J. Geophys. Res.* **114**, E00D03 (2009).
7. F. Billebaud *et al.*, *Planet. Space Sci.* **57**, 1446–1457 (2009).
8. G. Sindoni, V. Formisano, A. Geminale, *Planet. Space Sci.* **59**, 149–162 (2011).
9. V. A. Krasnopolsky, *Icarus* **190**, 93–102 (2007).
10. P. Hartogh *et al.*, *Astron. Astrophys.* **521**, L48 (2010).
11. P. Hartogh *et al.*, *Astron. Astrophys.* **521**, L49 (2010).
12. A. L. Sprague *et al.*, *Science* **306**, 1364–1367 (2004).
13. T. E. Economou, R. T. Pierrehumbert, paper presented at the 41st Lunar and Planetary Institute Science Conference, abstract 2179, The Woodlands, TX, 1 March 2010.
14. R. H. Becker, R. O. Pepin, *Earth Planet. Sci. Lett.* **69**, 225–242 (1984).
15. R. C. Wiens, R. H. Becker, R. O. Pepin, *Earth Planet. Sci. Lett.* **77**, 149–158 (1986).
16. K. Marti, J. S. Kim, A. N. Thakur, T. J. McCoy, K. Keil, *Science* **267**, 1981–1984 (1995).
17. H. C. Aoudjehane *et al.*, *Science* **338**, 785–788 (2012).

18. VPDB is a terrestrial isotopes standard.
19. P. B. Niles, W. V. Boynton, J. H. Hoffman, D. W. Ming, D. Hamara, *Science* **329**, 1334–1337 (2010).
20. V. A. Krasnopolsky, J. P. Maillard, T. C. Owen, R. A. Toth, M. D. Smith, *Icarus* **192**, 396–403 (2007).
21. D. D. Bogard, P. Johnson, *Science* **221**, 651–654 (1983).
22. R. H. Carr, M. M. Grady, I. P. Wright, C. T. Pillinger, *Nature* **314**, 248–250 (1985).
23. H. Y. McSween Jr., *Meteoritics* **29**, 757–779 (1994).
24. U. Ott, *Geochim. Cosmochim. Acta* **52**, 1937–1948 (1988).
25. U. Ott, F. Begemann, *Meteoritics* **20**, 721 (1985).
26. S. V. S. Murty, R. K. Mohapatra, *Geochim. Cosmochim. Acta* **61**, 5417–5428 (1997).
27. D. D. Bogard, D. H. Garrison, *Meteorit. Planet. Sci.* **33** (suppl.), 19 (1998).
28. A. H. Treiman, J. D. Gleason, D. D. Bogard, *Planet. Space Sci.* **48**, 1213–1230 (2000).
29. T. Owen, A. Bar-Nun, *AIP Conf. Proc.* **341**, 123–138 (1994).
30. T. D. Swindle, *AIP Conf. Proc.* **341**, 175 (1994).
31. T. D. Swindle, J. H. Jones, *J. Geophys. Res.* **102**, 1671 (1997).
32. Details of measurement procedures and treatment of uncertainties are provided in the supplementary materials on *Science* Online.
33. The turbomolecular pumps on SAM are expected to provide a more stable pressure of noble gas in the mass spectrometer ion source compared with the small ion pumps used on Viking.
34. C. R. Webster *et al.*, *Science* **341**, 260–263 (2013).
35. A. J. T. Jull, C. J. Eastoe, S. Cloudt, *J. Geophys. Res.* **102**, 1663 (1997).
36. B. M. Jakosky, R. O. Pepin, R. E. Johnson, J. L. Fox, *Icarus* **111**, 271–288 (1994).
37. D. H. Garrison, D. D. Bogard, *Meteorit. Planet. Sci.* **35** (suppl.), A58 (2000).
38. D. D. Bogard, R. N. Clayton, K. Marti, T. Owen, G. Turner, *Space Sci. Rev.* **96**, 425–458 (2001).
39. R. C. Wiens, R. O. Pepin, *Geochim. Cosmochim. Acta* **52**, 295–307 (1988).
40. D. Bogard, F. Horz, *Meteoritics* **21**, 337 (1986).
41. R. O. Pepin, *Nature* **317**, 473–475 (1985).
42. R. O. Pepin, *Icarus* **111**, 289–304 (1994).
43. T. Owen, A. Bar-Nun, *Icarus* **116**, 215–226 (1995).
44. P. R. Mahaffy *et al.*, *J. Geophys. Res. Planets* **105**, 15061–15071 (2000).
45. B. M. Jakosky, J. H. Jones, *Rev. Geophys.* **35**, 1–16 (1997).

Supplementary Materials

www.sciencemag.org/cgi/content/full/341/6143/263/DC1
Materials and Methods
Tables S1 and S2
References (*46*, *47*)
MSL Science Team Author List

18 March 2013; accepted 4 June 2013
10.1126/science.1237966

Ice-Shelf Melting Around Antarctica

E. Rignot,[1,2]* S. Jacobs,[3] J. Mouginot,[1] B. Scheuchl[1]

We compare the volume flux divergence of Antarctic ice shelves in 2007 and 2008 with 1979 to 2010 surface accumulation and 2003 to 2008 thinning to determine their rates of melting and mass balance. Basal melt of 1325 ± 235 gigatons per year (Gt/year) exceeds a calving flux of 1089 ± 139 Gt/year, making ice-shelf melting the largest ablation process in Antarctica. The giant cold-cavity Ross, Filchner, and Ronne ice shelves covering two-thirds of the total ice-shelf area account for only 15% of net melting. Half of the meltwater comes from 10 small, warm-cavity Southeast Pacific ice shelves occupying 8% of the area. A similar high melt/area ratio is found for six East Antarctic ice shelves, implying undocumented strong ocean thermal forcing on their deep grounding lines.

The Antarctic Ice Sheet and its 58-m sea level equivalent (*1*) is buttressed along most of its periphery by floating extensions of land ice called ice shelves and floating ice tongues (Fig. 1). Ice shelves cover an area >1.561 million km^2, comparable in size to the Greenland Ice Sheet, and fringe 75% of Antarctica's coastline while collecting 20% of its snowfall over 11% of its area (*2*, *3*). These features are nourished by the inflow of continental ice from grounded glaciers, surface accumulation, and freezing of marine ice on their undersides. They lose mass to iceberg calving and basal melting along with topside sublimation and wind drift. Ice shelves exert considerable control on glacier stability and Antarctic Ice Sheet mass balance (*4*–*6*) and play important roles in ocean stratification and bottom water formation (*7*).

The traditional view of ablation from Antarctic ice shelves has been that it occurs mostly by iceberg calving, with basal melting only contributing 10 to 28% of the total mass loss (*3*–*6*). Estimates of ice-shelf meltwater production derived from oceanographic data (*8*–*10*, e.g.) are impractical for synoptic circumpolar coverage. Numerical simulations of ice-ocean interactions extend from individual ice shelves to circumpolar models at various resolutions, but comparisons with observations are limited, and estimates of total ice-shelf meltwater production have varied from 357 to 1600 gigatons per year (1 Gt = 10^{12} kg) (*3*, *7*, *11*). Glaciological estimates have focused on few ice shelves (*6*, *12*, *13*) or near a fraction of glacier grounding lines (*14*) due to incomplete velocity and thickness mapping.

Here, we present more accurate, higher-resolution glaciological estimates of ice-shelf melting around the entire continent. At any point on an ice shelf of thickness H and velocity vector $\mathbf{v}$, the rate of ice-shelf thickening $\partial H/\partial t$ equals the sum of net surface mass balance *SMB* minus net basal melting B minus the lateral divergence in volume flux $H\mathbf{v}$ (*15*). A negative value of B indicates the freeze-on of marine ice. The calculation of volume flux divergence on a point per point basis yields the distribution of freeze/melt (Fig. 1). The integration of the total inflow and outflow within the ice-shelf perimeters yields the area-average melt rate and total meltwater production (Table 1).

For *SMB*, we use output products from the Regional Atmospheric and Climate Model RACMO2 (*16*), which is forced at the lateral boundary and sea surface by global reanalyses of the European Centre for Medium-Range Weather Forecasts. RACMO2 includes surface meltwater retention due to refreezing, evaporation, wind drift, and sublimation. The products have been validated with field data and an error propagation analysis (*17*) to a precision of 7 to 25%, average 10%, depending on location. We use the average *SMB* for the years 1979 to 2010 to represent a longer-term state.

Ice-shelf thickness is from Operation IceBridge (OIB) (*18*, *19*) and BEDMAP-2 (*1*) (fig. S1, supplementary materials). It combines direct measurements from radio-echo sounding, with indirect estimates from altimetry-derived ice-shelf surface elevation assuming hydrostatic equilibrium with a nominal precision of 15 to 50 m (*20*). Flux gates are selected at the location of Interferometric Synthetic Aperture Radar (InSAR)–derived grounding lines, which are more precise than those derived from photogrammetric techniques or visible imagery (*21*), with accompanying impacts on estimates of volume fluxes. Ice-front flux gates are at the seaward limit of the volume flux data, within 1 to 3 km of ice-front positions digitized from a 150-m spacing mosaic of Advanced Land Observing System (ALOS) Polarimetric SAR (PALSAR) data for the years 2007 and 2008.

Ice-shelf flow vector velocities are from InSAR data collected in 2007 and 2008 and processed at 450-m spacing (*22*). The average precision in speed is 4 m/year and 1.7° in direction (fig. S2). In the absence of vertical shear on floating ice, the surface-derived velocity is equivalent to a depth-averaged velocity. We surveyed 99.5% of Antarctic ice-shelf area in 2007 and 2008 (Table 1), or 1.554 million km^2, excluding a few smaller ice shelves where ice thickness is not well known (table S1). Drainage boundaries between ice shelves, including the eastern and western Ross, are defined by flow vector direction. Ice rises and islands are excluded from the ice-shelf area estimates but included in the *SMB* calculation.

Ice-shelf thickening $\partial H/\partial t$ for the period 2003 to 2008 is calculated using the procedure in (*23*), with an error dependent on firn depth corrections (fig. S3). The results are combined with *SMB* and the flux divergence to calculate B, with a precision dominated by uncertainties in

[1]Department of Earth System Science, University of California, Irvine, CA 92697, USA. [2]Jet Propulsion Laboratory, Pasadena, CA 91109, USA. [3]Lamont-Doherty Earth Observatory, Columbia University, Palisades, NY 10964, USA.

*Corresponding author. E-mail: erignot@uci.edu